Oxovanadium Pyrazole Complexes: Synthesis and Structure

Madan Mohan, Marcus R. Bond, Tom Otieno, and Carl J. Carrano*

Department of Chemistry, Southwest Texas State University, San Marcos, Texas 78666

Received July 29, 1994[⊗]

Aerial oxidation of acetonitrile solutions containing VCl_3 and pyrazole (pz), 3,5-dimethylpyrazole (3,5-Me_2pz), or 3(5)-*tert*-butylpyrazole (*t*-Bupz) in a 1:3 mole ratio, or potassium hydridotris(3(5)-*tert*-butylpyrazolyl)borate (K[HB(*t*-Bupz)$_3$]) in a 1:1 mole ratio, leads to the formation of a series of six-coordinate oxovanadium compounds. In the case of K[HB(*t*-Bupz)$_3$] a facile B−N bond cleavage is observed. The compounds isolated include $[(pz)_4VOCl]Cl\cdot H_2O$, **I**, $(3,5\text{-}Me_2pz)_2VOCl_2(H_2O)$, **II**, $(t\text{-}Bupz)_2VOCl_2$, **III**, $[(t\text{-}Bupz)_4VO(H_2O)]Cl_2\cdot 4CH_3CN$, **IV**, $(t\text{-}Bupz)_2VOCl_2(F)VOCl(t\text{-}Bupz)_3$, **V**, and $(t\text{-}Bupz)_2VO_2F$, **VI**. Compounds **V** and **VI** result from the treatment of **III** or **IV** with $AgBF_4$ or $AgPF_6$. All compounds have been characterized by spectroscopic methods, magnetic susceptibility measurements, and X-ray crystallography. Crystal data: **I**, triclinic, $P\bar{1}$, a = 8.629(2) Å, b = 8.666(1) Å, c = 15.064(2) Å, α = 106.13(1)°, β = 101.61(1)°, γ = 90.52(1)°, V = 1060.5(3) Å^3, Z = 2, T = 298 K, R = 7.91%, R_w = 9.88%; **II**, monoclinic, $C2/c$, a = 12.402(2) Å, b = 12.574(1) Å, c = 9.854(1) Å, β = 97.66(1)°, V = 1522.9(2) Å^3, Z = 4, T = 298 K, R = 3.22%, R_w = 5.15%; **III**, tetragonal, $P4_2/n$, a = 15.723(1) Å, c = 15.677(1) Å, V = 3875.6(5) Å^3, Z = 8, T = 298 K, R = 5.23%, R_w = 5.98%; **IV**, monoclinic, $C2$, a = 23.050(5) Å, b = 7.452(2) Å, c = 14.150(3) Å, β = 106.67(3)°, V = 2328.4(9) Å^3, Z = 2, T = 298 K, R = 5.74%, R_w = 7.76%; **V**, monoclinic, $P2_1/c$, a = 12.997(4) Å, b = 15.191(4) Å, c = 23.497(7) Å, β = 97.25(2)°, V = 4602(1) Å^3, Z = 4, T = 223 K, R = 3.80%, R_w = 3.60%; **VI**, tetragonal, $I4_1cd$, a = 15.116(1) Å, c = 32.698(3) Å, V = 7470.8(11) Å^3, Z = 16, T = 298 K, R = 6.40%, R_w = 7.35%. Steric effects and hydrogen bonding are important factors in determining the solid state structures of compounds in this family. In particular, compound **III** exists as a helical solid state polymer stabilized by intrachain hydrogen bonding.

Introduction

We have a continuing interest in exploring the effects of the steric character of pyrazole-derived ligands on the geometric structures and/or physicochemical properties of vanadium compounds.[1−4] Our studies of these compounds are also prompted by the anticipation that an understanding of their detailed structures may shed more light on the nature of histidine-containing binding sites in vanadoproteins and other metallobiomolecules. Although pyrazole complexes of vanadium(II) and -(III) have been known for some time,[5] little work appears to have been done with vanadium(IV) or -(V). While the vanadium(II) and -(III) pyrazole complexes are mononuclear with only small distortions from regular octahedral geometry, the pyrazole complexes of oxovanadium(IV) and -(V) have the potential to show some unusual structural features. The doubly bound oxo groups produce an inherently irregular coordination geometry in which the weakly bound trans ligands may be readily exchanged. In this situation the pyrazole ligands, with protonated and unprotonated nitrogens as ring neighbors, possess an intriguing potential for structural modification through secondary bonding interactions. Here the unprotonated nitrogen can coordinate the metal while leaving the hydrogen atom of the protonated nitrogen free to hydrogen-bond with appropriate ligands in its vicinity. Early synthetic results demonstrated a complicated descriptive chemistry for this family of compounds and prompted us to further investigate the synthetic and structural chemistry of these complexes. In this paper we report the synthesis and structural characterization of a number of new vanadium(IV) and -(V) compounds using pyrazole and its 3,5-dimethyl- and 3(5)-*tert*-butyl-substituted derivatives as ligands. By using pyrazoles of varying steric requirements, we have been able to investigate how this parameter affects the coordination chemistry at the vanadium center.

Experimental Section

Materials. Unless otherwise stated, all chemicals were reagent grade and were used as such without further purification. Solvents were dried and purified according to standard procedures. *t*-Bupz and K[HB(*t*-Bupz)$_3$] were synthesized and purified according to the reported procedures[6] and their authenticities checked by melting point and IR and proton NMR spectroscopies.

$[(pz)_4VOCl]Cl\cdot H_2O$, I. To vanadium trichloride (1.04 g, 6.61 mmol) was added 50 mL of acetonitrile (ACN) previously purged with nitrogen gas and the mixture refluxed at 85 °C for 0.75 h to give a dark green solution to which was added an acetonitrile solution (20 mL) of pyrazole (1.35 g, 19.8 mmol). The deep purple solution that resulted was stirred under nitrogen for 1 h and filtered to remove any unreacted materials. The filtrate was then stirred in the open atmosphere for an additional 2 h, during which time its color changed to green. The solution was then allowed to stand. Most of the solvent evaporated in about 2 weeks to give either thin purple plates of **I** or a blue viscous solution. Addition of 4 mL of methylene chloride and 10 mL of methanol to the viscous solution gave a green solution which, upon standing for an additional week, also yielded thin crystalline plates of compound **I**. Yield: 0.50 g (18%). Anal. Calcd for $C_{12}H_{18}N_8O_2Cl_2V$ (sample dried at 100 °C): C, 33.66; H, 4.24; N, 26.17; Cl, 16.56. Found: C, 33.95; H, 4.13; N, 26.25; Cl, 16.71. Vis [{solvent}, λ_{max}, cm^{-1} (ϵ, L mol^{-1} cm^{-1})]:

[⊗] Abstract published in *Advance ACS Abstracts,* February 1, 1995.

(1) Kime-Hunt, E.; Spartalian, K.; DeRusha, M.; Nunn, C. M.; Carrano, C. J. *Inorg. Chem.* **1989**, *28*, 4392.
(2) Holmes, S.; Carrano, C. J. *Inorg. Chem.* **1991**, *30*, 1231.
(3) Carrano, C. J.; Verastgue, R.; Bond, M. R. *Inorg. Chem.* **1993**, *32*, 3589.
(4) Mohan, M.; Holmes, S. M.; Butcher, R. J.; Jasinski, J. P.; Carrano, C. J. *Inorg. Chem.* **1992**, *31*, 2029.
(5) (a) Larkworthy, L. F.; O'Donoghue, M. W. *Inorg. Chim. Acta* **1983**, *71*, 81. (b) Karwecka, Z. *J. Coord. Chem.* **1979**, *9*, 37. (c) Mani, F. *Inorg. Nucl. Chem. Lett.* **1976**, *12*, 271. (d) Issigoni, M.; Katsaros, N.; Vrachnou-Astra, E.; Olympios, E. *Inorg. Chim. Acta* **1974**, *9*, 131.
(6) (a) Trofimenko, S.; Calabrese, J. C.; Thompson, J. S. *Inorg. Chem.* **1987**, *26*, 1507. (b) Calabrese, J. C.; Trofimenko, S.; Thompson, J. S. *J. Chem. Soc., Chem. Commun.* **1986**, 1122.

0020-1669/95/1334-1233$09.00/0

{MeOH}, 13 089 (26.19), ~16 667 (9.99); {DMF}, 12 626 (35.87), ~14 368 (26.68), 25 000 (53.69); {H_2O}, 13 193 (21.54), ~16 667 (10.44).

(3,5-Me_2pz)$_2$VOCl$_2$(H_2O), II. Vanadium trichloride (1.49 g, 9.47 mmol) and 3,5-dimethylpyrazole (2.74 g, 28.5 mmol) were treated in a manner similar to that used to prepare **I**, and the resultant green solution was allowed to stand. Blue crystals of the title compound and colorless crystals of 3,5-Me_2pz formed overnight. The solids were isolated by filtration and separated by washing with methylene chloride, in which only the uncomplexed ligand is soluble. Yield for **II**: 1.76 g (53%). Anal. Calcd for $C_{10}H_{18}N_4O_2Cl_2V$: C, 34.50; H, 5.21; N, 16.09. Found: C, 34.84; H, 5.23; N, 16.25. Vis [{solvent}, λ_{max}, cm^{-1} (ϵ, L mol^{-1} cm^{-1})]: {MeOH}, 12 563 (19.93), ~17 241 (8.51), ~25 641 (58.46); {DMF}, 12 563 (38.56), ~14 286 (29.00), 25 126 (38.51).

(*t*-Bupz)$_2$VOCl$_2$, III. To a solution of vanadium trichloride (5.0 g, 31.8 mmol) in 150 mL of acetonitrile was added with constant stirring an equimolar quantity of K[HB(*t*-Bupz)$_3$] (13.3 g, 31.4 mmol) or an excess of 3(5)-*tert*-butylpyrazole (11.8 g, 95.0 mmol). The resulting deep purple solution was stirred overnight. The solution was then exposed to air and stirred for an additional 8 h. During this period of time, the purple solution turned dark green and a green solid precipitated. The solid was removed by filtration, dried, and redissolved in hot acetonitrile. The resulting solution was filtered while hot, and the filtrate was slowly cooled to room-temperature to afford clusters of pale green needles. Yield: 4.5 g (36.7%). Mp: 213 °C. Anal. Calcd for $C_{14}H_{24}N_4OCl_2V$; C, 43.54; H, 6.26; N, 14.51, Cl, 18.36. Found: C, 43.53; H, 6.24; N, 14.56; Cl, 18.81. Vis [{solvent}, λ_{max}, cm^{-1} (ϵ, L mol^{-1} cm^{-1})]: {ACN}, 13 514 (35.75), 15 750 (33.14), 25 000 (22.66); {DMF}, 13 334 (31.84), 15 376 (20.60), 25 000 (47.56); {CH_2Cl_2}, 13 600 (28.00), 15 267 (34.10), 25 650 (23.34).

Crystals for X-ray analysis were obtained by thermal gradient recrystallization as follows. A 17-cm-long test tube containing a saturated acetonitrile solution of the above green product over an excess of the solid was placed in a heating block such that the lower end of the tube (≈4.5 cm) was at 37 °C and the upper end at room-temperature. X-ray quality crystals formed in the upper end of the tube and were harvested after a 3 month period.

[(*t*-Bupz)$_4$VO(H_2O)]Cl$_2$, IV. After removal of the green solid (**III**) by filtration, the filtrate was allowed to stand at room-temperature. After 24 h, a crop of purple crystals appeared and were shown by X-ray analysis to be [(*t*-Bupz)$_4$VO(H_2O)]Cl$_2$·CH_3CN. These were isolated by filtration, washed with diethyl ether, and air-dried. The crystals readily loose solvent to produce the unsolvated complex. Yield: 6.7 g (32.4%). Anal. Calcd for $C_{28}H_{50}N_8O_2Cl_2V$; C, 51.53; H, 7.72; N, 17.17. Found: C, 51.29; H, 7.71; N, 17.85. Vis [{solvent}, λ_{max}, cm^{-1} (ϵ, L mol^{-1} cm^{-1})]: {ACN}, 13 331 (38.77), 16 129 (25.90), 24 876 sh (14.49); {DMF}, 12 715 (32.02), 14 786 (19.87), 25 012 (76.20); {CH_2Cl_2}, 13 141 (38.60), 16 260 (20.54), 24 390 sh (14.22).

(*t*-Bupz)$_2$VOCl$_2$(F)VOCl(*t*-Bupz)$_3$, V. A solution of $AgBF_4$ (1.00 g, 5.20 mmol) in CH_2Cl_2 was added to a stirred solution of **III** (1.00 g, 2.59 mmol) in CH_2Cl_2 at room-temperature. A white precipitate (AgCl) formed immediately. The mixture was filtered and the filtrate evaporated to dryness under vacuum at room-temperature. The solid obtained was recrystallized from a CH_2Cl_2/hexane mixture at −20 °C and air-dried, giving **V** as blue crystals. Anal. Calcd for $C_{35}H_{60}N_{10}V_2O_2Cl_3F$; C, 47.78; H, 6.82; N, 15.91. Found: C, 48.19; H, 7.18; N, 16.13. Vis [{solvent}, λ_{max}, cm^{-1} (ϵ, L mol^{-1} cm^{-1})]: {ACN}, 13 334 (67.93), 15 875 (42.65), 24 875 w, sh (11.06); {DMF}, 13 334 (67.93), 15 385 (37.63), 25 000 w, sh (6.72); {CH_2Cl_2}, 13 334 (54.71), 15 750 (32.57), 24 690 w, sh (6.50).

Physical Measurements. Elemental analyses were performed by Desert Analytics, Tucson, AZ. Infrared spectra were obtained on a Perkin-Elmer 1600 FT-IR spectrometer as KBr pellets. UV−vis spectra were recorded on either a Perkin-Elmer 553 or an HP 8520 diode array spectrophotometer. EPR spectra were recorded on either an IBM Bruker ER-300 or a MicroNow 8300A X-band spectrometer with temperature regulated by a variable-temperature cryostat. Operating conditions are as described in figure captions. Quartz flat cells were used for polar solvents, and cylindrical quartz tubes were employed for nonpolar solvents and frozen mixed solvents.

Routine room-temperature solid state susceptibilities were measured using a Johnson-Mathey MSB-1 susceptibility balance. Solution susceptibility data were obtained at room-temperature via the Evans method and employed a Bruker NR80 FT NMR spectrometer. Variable-temperature magnetic susceptibilities were measured in the temperature range 5−270 K on an LDJ 9600 vibrating-sample magnetometer. Finely ground samples were packed and sealed in a gelatin capsule sample holder. Temperature was controlled by using an Oxford ITC4 set-point temperature controller and cryostat. Temperature was measured with a thermocouple located approximately 1.5 cm from the sample and upstream with respect to the direction of the flow of the coolant gas. The magnetic moment was calibrated to the saturation moment of a nickel metal standard. Temperature calibration was checked using the magnetic standards $HgCo(SCN)_4$ and $[(CH_3)_2NHCH_2]_2CuCl_4$. Temperature-independent contributions to the paramagnetism were accounted for through an empirical correction obtained from a plot of χ_{raw} versus $1/T$ for **V** or by utilizing Pascal's constants for the diamagnetism in **III**. A TIP correction was applied in the model used for **III**.

X-ray Data Collection and Analysis. Crystals were mounted in Lindemann glass capillaries and data collected using a Siemens P4 diffractometer for compounds **I**−**IV** and **VI**. Crystals of **V** were observed to decompose following removal from the mother liquor; hence the crystal used in the analysis was rapidly transferred to a goniometer and placed in a stream of dry nitrogen gas at −50 °C on a Nicolet R3 m/V diffractometer. Preliminary diffractometer data and/or axial photography led to unit cell choices. Following accurate centering of 20−30 relatively high angle reflections, intensity data were collected. Structure solution and refinement were achieved using the SHELXTL-PLUS crystallographic software[7] from Siemens. The Patterson method was used to solve the structures of **I** and **II**, and direct-method procedures were used for **III**−**VI**. Hydrogen positions were generally calculated to give an idealized geometry and fixed to ride on their respective bound atoms with fixed, isotropic thermal parameters. No corrections were made for the presence of extinction in any of the compounds. Crystal data are given in Table 1, and final atomic parameters for compounds **I**−**VI** are given in Tables 2−7, respectively.

The chloride counterion in **I** was found to be disordered over two positions and occupancy factors were refined. The total occupancy of the chloride was constrained to unity on the basis of both charge considerations and the microanalytical results. Crystallographically, the water of hydration in this compound (whose presence was also indicated by microanalytical and infrared spectral data), was found to be disordered with four positions eventually being identified; occupancy factors were again refined. The space group for **III**, $P4_2/n$ is uniquely determined by the reflection conditions $00l$, $l = 2n$ and $hk0$, $h + k = 2n$. The $4L$ repeat unit of the chain structure in **III**, however, produces the additional reflection condition $00l$, $l = 4n$. No space group matches this broader set of conditions, and the last condition is weakly violated. Hence $P4_2/n$ was chosen as the correct space group, a fact confirmed by the successful refinement. In the case of **IV**, systematic absences led to three possible space group choices: $C2$, $C2/m$, and Cm. The statistics clearly favored a noncentric space group (0.754 found and 0.736 expected for $|E^2 - 1|$). Of the noncentric possibilities, $C2$ is far the more common and was thus chosen for an initial evaluation. The successful refinement in $C2$ validated this choice. An absolute structure parameter was refined for structure **IV**. The value obtained, 2.1(5), indicates that the reported structure is probably the correct enantiomer, although the large esd suggests that this feature is not well determined. Two distinct crystal isomorphs were observed for **V**, octahedral crystals which proved to be twinned and flat plates which rapidly deteriorated in the absence of solvent. A bright blue block having approximate dimensions of 0.7 × 0.3 × 0.2 mm was cut from a much larger slab of the latter and was rapidly mounted on the goniometer and placed in a stream of dry nitrogen gas at −50 °C. One of the *tert*-butyl groups was found to be heavily disordered with three major orientations eventually being identified. This was modeled as three ideal rigid-body groups, each allowed to rotate independently. On the basis of the analysis of the isotropic temperature factors involved, the population factors used were 0.45, 0.25, and 0.30 for C(11), C(11′), and C(11″) groups (*vide infra*), respectively.

(7) Sheldrick, G. M. *SHELXTL-PC, Version 4.1*; Siemens X-ray Analytical Instruments, Inc.: Madison, WI, 1989. Scattering factors from: *International Tables for X-ray Crystallography*; Ibers, J., Hamilton, W., Eds.; Kynoch: Birmingham, England, 1974; Vol. IV.

Table 1. Crystallographic Data for Compounds **I**–**VI**[a,b]

	I	II	III
formula	$C_{12}H_{18}N_8O_2Cl_2V$	$C_{10}H_{18}N_4O_2Cl_2V$	$C_{14}H_{24}N_4OCl_2V$
fw	428.2	348.1	386.2
space group	$P\bar{1}$ (No. 2)	$C2/c$ (No. 15)	$P4_2/n$ (No. 86)
a, Å	8.629(2)	12.402(2)	15.723(1)
b, Å	8.666(1)	12.574(1)	15.723(1)
c, Å	15.064(2)	9.854(1)	15.677(1)
α, deg	106.13(1)	90	90
β, deg	101.61(1)	97.66(1)	90
γ, deg	90.52(1)	90	90
V, Å^3	1060.5(3)	1522.9(2)	3875.6(5)
Z	2	4	8
ϱ_{calcd}, g cm^{-3}	1.338	1.518	1.324
μ, cm^{-1}	7.42	10.05	7.93
T, °C	25	25	25
radiation (λ, Å)	Mo Kα (0.710 73)	Mo Kα (0.710 73)	Mo Kα (0.710 73)
R, %	7.91	3.22	5.23
R_w, %	9.88	5.15	5.98

	IV	V	VI
formula	$C_{36}H_{62}N_{12}O_2Cl_2V$	$C_{35}H_{60}N_{10}O_2FCl_2V_2$	$C_{14}H_{24}N_4O_2FV$
fw	816.8	880.3	350.3
space group	$C2$ (No. 5)	$P2_1/c$ (No. 14)	$I4_1cd$ (No. 110)
a, Å	23.050(5)	12.997(4)	15.116(1)
b, Å	7.452(2)	15.191(4)	15.116(1)
c, Å	14.150(3)	23.497(7)	32.698(3)
β, deg	106.67(3)	97.25(2)	90
V, Å^3	2328.4(9)	4602(1)	7470.8(11)
Z	2	4	16
ϱ_{calcd}, g cm^{-3}	1.164	1.27	1.246
μ, cm^{-1}	3.7	6.11	5.51
T, °C	25	−50	25
radiation (λ, Å)	Mo Kα (0.710 73)	Mo Kα (0.710 73)	Mo Kα (0.710 73)
R, %	5.74	3.80	6.40
R_w, %	7.76	3.60	7.35

[a] Estimated standard deviations in the least significant digit are given in parentheses. [b] Quantity minimized = $\sum w(F_o - F_c)^2$, $w = [\sigma^2(F) + 0.0008F^2]^{-1}$, $R = \sum|(F_o - F_c)|/\sum F_o$, and $R_w = (\sum(w(F_o - F_c)^2/\sum(wF_o)^2))^{1/2}$.

Results

Synthesis. Reaction of VCl_3 with pyrazole, 3,5-dimethylpyrazole or 3(5)-*tert*-butylpyrazole in a 1:3 mole ratio (or with an equimolar quantity of K[HB(*t*-Bupz)$_3$]) in acetonitrile under an inert atmosphere results in formation of deep purple solutions. These solutions have optical spectra very similar to that of the crystallographically characterized, linear, oxo-bridged vanadium(III) dimer $[HB(pz)_3H_2B(pz)_2V]_2O$, the intense optical bands of which are due to LMCT transitions associated with the $[V-O-V]^{4+}$ core.[8] Hence, the initial species formed in the pyrazole reactions is probably a linear oxo-bridged vanadium(III) tris(pyrazole) complex. Exposing these solutions to air results in oxidation and the formation of crystalline oxovanadium(IV) compounds. The vanadyl oxygen atoms presumably come from water or molecular oxygen.

$[(pz)_4VOCl]Cl\cdot H_2O$, I. X-ray analysis of the crystalline plates obtained for **I** indicates that it is a six-coordinate mononuclear oxovanadium(IV) compound. The four pyrazole ligands occupy the equatorial coordination sites of the vanadium, the axial sites being occupied by a vanadyl oxygen atom and a chlorine atom. A chloride ion and a water molecule occupy sites outside the coordination sphere of the vandium. Figure 1 shows the atom-labeling scheme for the cationic portion of **I**. The V=O, V–Cl, and mean V–N bond lengths are 1.619(7), 2.465(3), and 2.121(9) Å, respectively. The *cis* L–V–L angles, where L represents the donor atoms bonded to the vanadium, all lie within the range 86–94° whereas the Cl–V–O and the mean *trans* N–V–N angles are 179.5(3) and 173.9(3)°, respectively. The chloride ion and the free amino hydrogen on the pyrazole rings form strong hydrogen bonds (Cl···H average ca 2.4 Å and H···Cl···H average 175°), which serve to weakly link two adjacent molecules together. The lattice water molecules also appear to contribute to this hydrogen-bonding network; however the disorder in the position of the chloride counterion and associated water of hydration (see Experimental Section) reduce the overall accuracy of the structure and we are unable to provide further details.

The V=O stretching infrared absorption, $\nu_{V=O}$, for **I** found at 977 cm^{-1} is within the 935–1035 cm^{-1} range as expected for a simple vanadyl(IV) species.[9] A solution of **I** in water exhibits an eight-line EPR spectrum at room-temperature whereas, in a water/glycerine mixture at 77 K, an axially symmetric anisotropic spectrum is observed. These features are characteristic of a mononuclear vanadium(IV) compound and are consistent with the X-ray structural data.

Table 2. Atomic Coordinates ($\times 10^4$) and Equivalent Isotropic Displacement Coefficients (Å^2 × 10^3) for **I**[a]

	x	y	z	U_{eq}
V(1)	1974(2)	711(2)	2888(1)	42(1)
Cl(1)	3054(3)	1169(4)	4592(2)	63(1)
N(8)	4124(9)	−320(10)	2675(5)	47(3)
N(7)	3043(9)	3017(10)	3028(6)	47(4)
N(6)	999(9)	−1529(10)	2897(6)	49(4)
C(3)	5321(10)	−558(12)	3326(6)	39(4)
O(1)	1259(7)	396(8)	1769(4)	51(3)
N(4)	−82(9)	1816(10)	3269(6)	50(4)
N(3)	−1316(10)	1996(11)	2609(7)	62(4)
C(9)	826(13)	−2172(14)	3569(8)	65(5)
C(8)	3710(13)	4225(13)	3759(8)	59(5)
C(12)	−484(14)	2480(14)	4079(8)	68(5)
C(11)	−2486(14)	2684(15)	2989(11)	76(7)
C(10)	6455(13)	−1342(16)	2933(10)	74(6)
N(2)	313(11)	−2646(12)	2078(7)	69(5)
N(1)	3133(10)	3488(11)	2278(6)	60(4)
C(7)	3839(13)	4977(15)	2517(10)	71(6)
C(6)	6042(14)	−1584(16)	1997(10)	81(7)
C(5)	4260(13)	5460(14)	3483(10)	74(6)
C(4)	−233(14)	−3942(14)	2270(10)	74(6)
N(5)	4528(14)	−948(14)	1849(8)	94(6)
C(2)	−2002(15)	3021(16)	3929(12)	85(7)
C(1)	99(14)	−3735(14)	3180(10)	73(6)
Cl(2B)[b]	−2230(15)	1488(20)	579(6)	233(9)
Cl(2A)[b]	−1236(37)	−2633(23)	−93(9)	209(14)
O(2B)[b]	3201(103)	1703(48)	390(23)	166(47)
O(2A)[b]	−633(83)	3200(47)	−222(22)	144(28)
O(2D)[b]	5877(85)	3783(124)	533(37)	363(60)
O(2C)[b]	4715(239)	4546(181)	299(74)	232(98)

[a] Equivalent isotropic U defined as one-third of the trace of the orthogonalized U_{ij} tensor. [b] Occupancy factors for Cl(2B) 0.578, Cl(2A) 0.421, O(2B) 0.269, O(2A) 0.231, O(2D) 0.339, O(2C) 0.161.

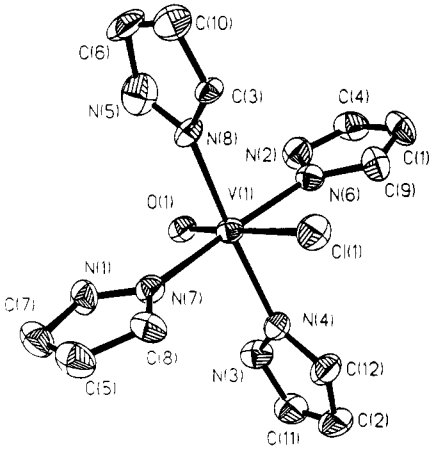

Figure 1. Thermal ellipsoid plot (30%) for **I** with atom-labeling scheme.

(8) Carrano, C. J. Unpublished results.

(9) Selbin, J. *Chem. Rev.* **1965**, *65*, 153.

Table 3. Atomic Coordinates ($\times 10^4$) and Equivalent Isotropic Displacement Coefficients ($Å^2 \times 10^3$) for **II**[a]

	x	y	z	U_{eq}
V(1)	5000	3331(1)	2500	26(1)
Cl(2)	5525(1)	3603(1)	280(1)	33(1)
O(1)	5000	2072(2)	2500	40(1)
O(2)	5000	5135(2)	2500	34(1)
N(1)	3348(2)	3549(2)	1632(2)	31(1)
N(2)	3031(2)	4351(2)	735(2)	34(1)
C(1)	1960(2)	4329(2)	301(3)	37(1)
C(2)	1556(2)	3478(2)	938(3)	41(1)
C(3)	2426(2)	3016(2)	1763(3)	34(1)
C(4)	2413(3)	2074(3)	2683(3)	50(1)
C(5)	1437(3)	5135(3)	−677(4)	57(1)

[a] Equivalent isotropic U defined as one-third of the trace of the orthogonalized $\mathbf{U}_{ij}$ tensor.

Table 4. Atomic Coordinates ($\times 10^4$) and Equivalent Isotropic Displacement Coefficients ($Å^2 \times 10^3$) for **III**[a]

	x	y	z	U_{eq}
V(1)	2500	7500	85(1)	25(1)
V(2)	2500	7500	−2420(1)	25(1)
Cl(1)	3097(2)	6153(2)	−162(1)	39(1)
Cl(2)	3064(2)	8862(2)	−2655(1)	38(1)
O(1)	2500	7500	1109(4)	29(3)
O(2)	2500	7500	−1394(4)	32(3)
N(11)	3716(4)	8044(5)	−19(4)	26(2)
N(12)	4337(4)	7928(5)	578(4)	36(3)
C(11)	4068(6)	8573(6)	−577(6)	40(4)
C(12)	4871(7)	8789(7)	−347(6)	54(4)
C(13)	5054(6)	8367(6)	402(6)	38(4)
C(130)	5809(6)	8373(7)	982(7)	47(4)
C(131)	6571(7)	8756(10)	500(8)	111(7)
C(132)	6057(7)	7489(8)	1266(7)	79(6)
C(133)	5612(8)	8911(9)	1736(8)	111(7)
N(21)	3722(4)	6982(4)	−2567(4)	29(3)
N(22)	4101(5)	6538(5)	−1927(4)	38(3)
C(21)	4270(6)	6979(6)	−3198(6)	36(3)
C(22)	5007(6)	6575(6)	−2986(6)	35(4)
C(23)	4902(6)	6297(6)	−2161(6)	41(4)
C(230)	5467(7)	5816(8)	−1529(6)	61(5)
C(231)	6287(8)	5606(11)	−1958(9)	154(10)
C(232)	5024(9)	4984(8)	−1243(7)	92(6)
C(233)	5605(8)	6347(9)	−725(8)	96(6)

[a] Equivalent isotropic U defined as one-third of the trace of the orthogonalized $\mathbf{U}_{ij}$ tensor.

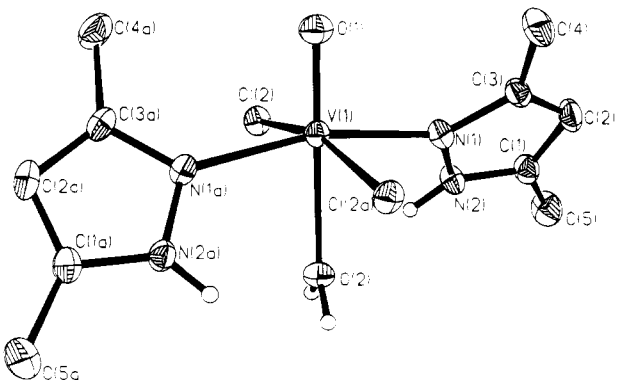

Figure 2. Thermal ellipsoid plot (30%) for **II** with atom-labeling scheme.

(3,5-Me$_2$pz)$_2$VOCl$_2$(H$_2$O), II. The crystal data and selected bonding parameters for **II** are given in Tables 1 and 8, respectively. Its structure, with the atom-labeling scheme, is depicted in Figure 2. Six-coordination of the vanadium is achieved through two *trans*-nitrogen atoms from the two 3,5-Me$_2$pz ligands, two *trans*-chlorine atoms, an oxo oxygen, and a water oxygen. The molecule has a formal C_2 symmetry with the axis coincident with the V=O bond. Bond lengths and angles around the vanadium are unexceptional. As expected,

Table 5. Atomic Coordinates ($\times 10^4$) and Equivalent Isotropic Displacement Coefficients ($Å^2 \times 10^3$) for **IV**[a]

	x	y	z	U_{eq}
V(1)	0	4242	0	31(1)
Cl(1)	−216(1)	8990(4)	−1808(1)	49(1)
O(1)	0	6362(12)	0	38(3)
O(2)	0	1376(12)	0	41(3)
N(1)	−539(3)	4060(12)	983(4)	36(2)
N(2)	−618(3)	5504(12)	1530(5)	41(3)
N(3)	−781(3)	4008(11)	−1232(4)	36(2)
N(4)	−971(3)	5388(11)	−1884(5)	42(3)
N(5)	1071(9)	1532(29)	5394(14)	165(10)
N(6)	2855(5)	5401(24)	−457(10)	124(7)
C(1)	−869(4)	2794(15)	1200(7)	46(4)
C(2)	−1169(5)	3391(13)	1873(8)	47(4)
C(3)	−989(4)	5124(14)	2085(6)	39(3)
C(31)	−1145(4)	6505(14)	2768(7)	50(4)
C(32)	−1671(5)	5779(18)	3109(8)	73(5)
C(33)	−598(5)	6773(17)	3667(8)	74(5)
C(34)	−1325(6)	8307(14)	2234(8)	70(5)
C(4)	−1170(4)	2686(14)	−1563(7)	48(4)
C(5)	−1618(5)	3228(14)	−2423(8)	57(4)
C(6)	−1476(4)	4934(13)	−2600(7)	44(4)
C(61)	−1776(5)	6229(15)	−3436(7)	61(4)
C(62)	−2322(6)	5317(24)	−4125(10)	130(7)
C(63)	−1950(6)	7934(20)	−2998(9)	97(6)
C(64)	−1332(6)	6733(19)	−4014(8)	88(6)
C(7)	326(7)	2163(22)	3682(11)	112(8)
C(8)	751(9)	1794(23)	4636(14)	104(8)
C(9)	2501(7)	5565(22)	−50(11)	80(5)
C(10)	2074(7)	5673(24)	504(10)	108(7)

[a] Equivalent isotropic U defined as one-third of the trace of the orthogonalized $\mathbf{U}_{ij}$ tensor.

the V−OH$_2$ bond *trans* to the oxo group is lengthened (2.268 Å) relative to other vanadium(IV)−aquo bonds where the water is *cis* to the vanadyl unit (ca. 2.08 Å).[10] The two 3,5-Me$_2$pz rings are planar within experimental error and are tilted by about 37°, to opposite sides, from the V=O axis. The dihedral angle between the planes defined by the two rings is 72.7°. Each chlorine atom is involved in intermolecular H-bonding with a water hydrogen atom and an NH hydrogen from a neighboring molecule.

The $\nu_{V=O}$ for **II** (991 cm^{-1}) falls within the expected range, and its EPR spectra in methanol (room-temperature) and methanol/toluene (77 K) are similar to those of **I** and consistent with the structure of **II** as established by X-ray crystallography.

(*t*-Bupz)$_2$VOCl$_2$, III. In the case of the *tert*-butylpyrazole ligand, exposing the deep purple solution to the air resulted in the precipitation of fine green needles. Elemental analysis gave an empirical formula of (*t*-Bupz)$_2$VOCl$_2$. In a variety of solvents, the green solid dissolves to give blue solutions, the optical, room-temperature EPR, and IR ($\nu_{V=O}$ at 955 cm^{-1}) spectra and magnetic moment (Evans method, $\mu_{eff} = 1.78\ \mu_B$) of which are characteristic of a simple square pyramidal vanadyl complex. Its conductivity in acetonitrile or DMF is consistent with a 2:1 electrolyte, indicating dissociation of the chlorides in polar solutions.

The change in color on going from the solid state to solution suggested that some sort of solid state interaction was occurring. This was confirmed by the absence of the normal $\nu_{V=O}$ between 935 and 1035 cm^{-1} in the solid state IR and its appearance as an intense band at 880 cm^{-1}. Such a low V=O stretching frequency has been associated with head-to-tail solid state polymerization.[11-16] The formation of a solid state polymer is

(10) (a) Bukovec, P.; Milicev, S.; Demsar, A.; Golic, L. *J. Chem. Soc., Dalton Trans.* **1981**, 1802. (b) Priebsch, W.; Rehder, D. *Inorg. Chem.* **1990**, *29*, 3013.
(11) Mathew, M.; Carty, A. J.; Palenik, G. J. *J. Am. Chem. Soc.* **1970**, *92*, 3197.
(12) Farmer, R. L.; Urbach, F. L. *Chem. Commun.* **1970**, 1515.

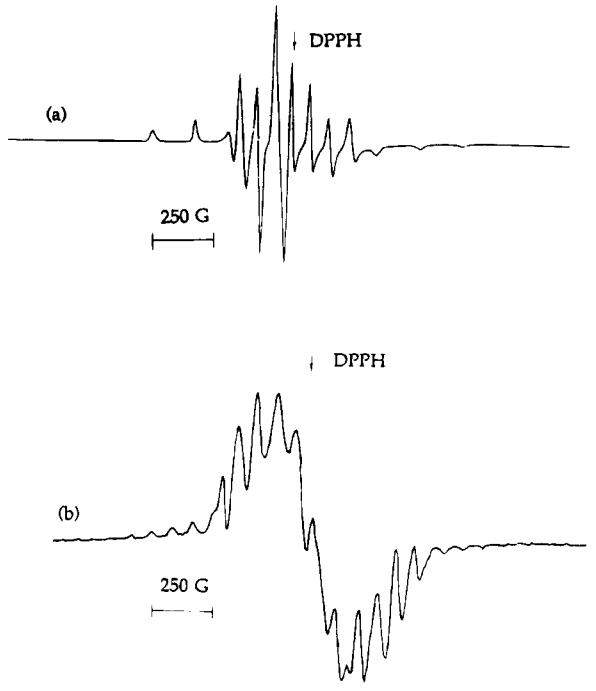

Figure 3. X-band EPR spectra of **III**: (a) frozen methanol, 115 K; (b) frozen CH_2Cl_2/toluene glass, 115 K. Conditions: 9.43 GHz frequency, 2 mW power, 4.0 G modulation amplitude, 2.5×10^3 gain, 2500 G scan range, 1.5 min scan time.

also supported by the variable-temperature magnetochemistry and frozen-solution EPR.

At room-temperature, compound **III** in CH_2Cl_2 or a host of other solvents, exhibits an eight-line EPR spectrum characteristic of a mononuclear vanadium ($I = {}^7/_2$) complex. In good coordinating solvents such as DMF, CH_3CN, or MeOH, freezing the solution (115 K) yields an axially symmetric anisotropic spectrum (Figure 3a). However, in the poorly coordinating CH_2Cl_2 or CH_2Cl_2/toluene a more complicated (≈20 line) spectrum (Figure 3b) with a set of faint peaks at approximately half the resonance field is observed, with the color changing from blue to green upon freezing. This EPR spectrum is characteristic of a dinuclear vanadium(IV) compound.[17a] The EPR spectrum was thus interpreted using the following spin Hamiltonian for a dimeric compound with $S = 1$ and $I = {}^7/_2$: $\mathcal{H} = g_{\parallel}\mu_B H_z S_z + g_{\perp}\mu_B H_x S_x + g_{\perp}\mu_B H_y S_y + D[S_z^2 - S(S+1)/3] + A_{\parallel} S_z I_z + A_{\perp} S_x I_x + A_{\perp} S_y I_y$, where D is the zero-field splitting parameter and all the other symbols have their usual meanings. The term containing D was omitted in the analysis of the room-temperature spectrum of this compound as well as spectra of the mononuclear compounds. Experimental conditions and values of the parameters obtained are given in figure captions and in Table 9. The main portion of the spectrum consists of overlapping high- and low-field transitions taken parallel and perpendicular to the chain axis that result from a small zero-field splitting (D) in the spin triplet of the dimer. Measurements in the parallel region yield a value of $D = 0.0186$ cm^{-1} which, assuming D is exclusively dipolar in origin, corresponds to an intradimer V···V distance, R, of 5.12 Å.[17b] Each transition envelope appears to contain the uniformly spaced 15-line hyperfine spectrum expected for a vanadium dimer with a significant amount of isotropic magnetic exchange. As discussed earlier, infrared spectral studies indicate that the polymeric structure of **III** breaks down in solution. The EPR spectral data presented here suggest that, in frozen solutions containing nonpolar solvents, the compound adopts a dimeric structure. Spectra of the crystalline solid measured at −180 and +20 °C also indicate the presence of isotropic exchange.

Table 6. Atomic Coordinates ($\times 10^4$) and Equivalent Isotropic Displacement Coefficients (Å^2 × 10^3) for **V**[a]

	x	y	z	U_{eq}
V(1)	2504(1)	7849(1)	3107(1)	29(1)
V(2)	3459(1)	5362(1)	3689(1)	30(1)
Cl(1)	1265(1)	7773(1)	3770(1)	42(1)
Cl(2)	3341(1)	5083(1)	2679(1)	42(1)
Cl(3)	5167(1)	5917(1)	3708(1)	43(1)
F	2933(2)	6624(1)	3414(1)	33(1)
O(1)	2184(2)	8803(2)	2869(1)	39(1)
O(2)	3767(2)	4402(2)	3918(1)	41(1)
N(1)	3651(3)	8323(2)	3756(1)	33(1)
N(2)	4566(3)	7932(2)	3945(2)	35(1)
N(3)	3711(3)	7766(2)	2591(1)	33(1)
N(4)	4344(3)	7094(2)	2483(2)	36(1)
N(5)	1452(3)	7211(2)	2478(1)	31(1)
N(6)	1410(3)	6349(2)	2316(2)	33(1)
N(7)	3372(3)	5877(2)	4519(1)	33(1)
N(8)	2905(3)	6633(2)	4656(2)	35(1)
N(9)	1856(3)	5058(2)	3673(1)	36(1)
N(10)	1026(3)	5607(2)	3661(2)	36(1)
C(1)	3754(4)	9138(3)	3957(2)	42(2)
C(2)	4724(4)	9263(3)	4271(2)	47(2)
C(3)	5236(3)	8472(3)	4255(2)	40(2)
C(4)	6318(3)	8197(3)	4492(2)	54(2)
C(5)	6859(4)	8958(4)	4832(3)	90(3)
C(6)	6913(4)	7965(4)	3991(3)	78(2)
C(7)	6280(4)	7407(4)	4890(2)	77(2)
C(8)	4100(3)	8476(3)	2351(2)	46(2)
C(9)	4965(4)	8245(3)	2096(2)	50(2)
C(10)	5115(3)	7361(3)	2187(2)	38(2)
C(11)	6001(6)	6825(6)	2019(3)	53(2)
C(12)	7014	7316	2199	53(2)
C(13)	5827	6743	1367	53(2)
C(14)	6062	5910	2287	53(2)
C(11′)	5929(9)	6732(8)	2010(6)	64(4)
C(12′)	6892	6893	2439	64(4)
C(13′)	6180	6922	1405	64(4)
C(14′)	5588	5776	2049	64(4)
C(11″)	5876(10)	6732(8)	1962(4)	56(3)
C(12″)	6842	7247	1860	56(3)
C(13″)	5380	6332	1398	56(3)
C(14″)	6177	5999	2395	56(3)
C(15)	626(3)	7578(3)	2177(2)	40(2)
C(16)	66(3)	6965(3)	1828(2)	42(2)
C(17)	588(3)	6178(3)	1920(2)	34(2)
C(18)	372(3)	5272(3)	1668(2)	41(2)
C(19)	1198(4)	5022(3)	1290(2)	67(2)
C(20)	−694(4)	5276(3)	1314(2)	73(2)
C(21)	384(4)	4590(3)	2151(2)	55(2)
C(22)	3742(3)	5530(3)	5025(2)	43(2)
C(23)	3511(3)	6056(3)	5474(2)	44(2)
C(24)	2965(3)	6758(3)	5228(2)	36(2)
C(25)	2457(3)	7537(3)	5479(2)	41(2)
C(26)	2725(4)	7528(3)	6133(2)	60(2)
C(27)	1266(3)	7466(3)	5335(2)	55(2)
C(28)	2825(4)	8396(3)	5235(2)	62(2)
C(29)	1472(4)	4258(3)	3750(2)	45(2)
C(30)	411(3)	4309(3)	3788(2)	46(2)
C(31)	146(3)	5180(3)	3730(2)	36(2)
C(32)	−877(3)	5639(3)	3748(2)	48(2)
C(33)	−1750(4)	4980(4)	3593(3)	85(3)
C(34)	−1019(4)	6384(4)	3309(3)	86(3)
C(35)	−914(4)	5982(5)	4342(3)	106(3)

[a] Equivalent isotropic U defined as one-third of the trace of the orthogonalized U_{ij} tensor.

(13) McCormick, B. J.; Bozis, R. A. *Inorg. Chem.* **1971**, *10*, 2806.
(14) Mannix, C. E.; Zipp, A. P. *J. Inorg. Nucl. Chem.* **1979**, *41*, 59.
(15) Al-Niaimi, N. S.; Al-Karaghouli, A. R.; Aliwi, S. M.; Jalhoom, M. G. *J. Inorg. Nucl. Chem.* **1974**, *36*, 283.
(16) Hamilton, D. E. *Inorg. Chem.* **1991**, *30*, 1670.
(17) (a) Thanabal, V.; Krishnan, V. *Inorg. Chem.* **1982**, *21*, 3606. (b) For an oxovanadium(IV) complex the sets of EPR lines in the perpendicular region are separated by D while the parallel sets are separated by 2D. Thus D can be determined directly from the spectrum and then, for an axial dimer, R calculated using the equation $R = (0.65g^2/D)^{1/3}$. See ref 17a.

Table 7. Atomic Coordinates ($\times 10^4$) and Equivalent Isotropic Displacement Coefficients ($Å^2 \times 10^3$) for **VI**[a]

	x	y	z	U_{eq}
V(1)	3564(1)	76(2)	3700	58(1)
F(1)	2118(4)	130(4)	3739(5)	46(2)
N(11)	3476(9)	−1116(8)	4043(5)	59(5)
O(2)	4132(8)	−430(7)	3343(3)	65(4)
N(12)	4247(9)	−1469(10)	4205(5)	58(5)
O(1)	4184(8)	535(7)	4080(4)	81(5)
N(22)	4351(10)	1559(9)	3222(5)	54(5)
C(21)	4354(13)	2396(12)	3042(6)	53(6)
N(21)	3631(10)	1259(8)	3389(4)	53(5)
C(12)	3190(11)	−2457(12)	4290(7)	69(7)
C(11)	4070(12)	−2289(11)	4346(6)	54(6)
C(23)	3051(13)	1926(13)	3334(7)	79(7)
C(110)	4779(16)	−2825(15)	4567(7)	78(9)
C(22)	3484(15)	2587(12)	3122(7)	84(8)
C(13)	2857(13)	−1732(13)	4108(7)	75(7)
C(210)	5086(10)	2864(12)	2871(6)	78(9)
C(111)	4415(16)	−3738(13)	4711(10)	154(12)
C(113)	4984(23)	−2405(18)	4985(9)	198(14)
C(211)	5783(19)	2291(16)	2765(10)	272(16)
C(212)	5375(19)	3457(19)	3174(9)	278(16)
C(112)	5603(17)	−2848(25)	4284(10)	216(14)
C(213)	4817(16)	3340(23)	2523(8)	389(16)

[a] Equivalent isotropic U defined as one-third of the trace of the orthogonalized $\mathbf{U}_{ij}$ tensor.

Table 8. Selected Bond Lengths (Å) and Bond Angles (deg) for **II** and **III**[a]

Compound **II**			
V(1)−Cl(2)	2.388(1)	V(1)−O(1)	1.584(3)
V(1)−O(2)	2.268(3)	V(1)−N(1)	2.130(2)
V(1)−Cl(2A)	2.388(1)	V(1)−N(1A)	2.130(2)
Cl(2)−V(1)−O(1)	98.2(1)	Cl(2)−V(1)−O(2)	81.8(1)
O(1)−V(1)−O(2)	180	Cl(2)−V(1)−N(1)	88.8(1)
O(1)−V(1)−N(1)	97.4(1)	O(2)−V(1)−N(1)	82.6(1)
Cl(2)−V(1)−Cl(2A)	163.6(1)	O(1)−V(1)−Cl(2A)	98.2(1)
O(2)−V(1)−Cl(2A)	81.8(1)	N(1)−V(1)−Cl(2A)	89.1(1)
Cl(2)−V(1)−N(1A)	89.1(1)	O(1)−V(1)−N(1A)	97.4(1)
O(2)−V(1)−N(1A)	82.6(1)	N(1)−V(1)−N(1A)	165.3(1)
Cl(2A)−V(1)−N(1A)	88.8(1)		
Compound **III**			
V(1)−Cl(1)	2.349(2)	V(2)−Cl(2)	2.346(2)
V(1)−O(1)	1.606(7)	V(2)−O(2)	1.607(7)
V(1)−O(2)	2.319(7)	V(2)−O(1A)	2.306(7)
V(1)−N(11)	2.101(7)	V(2)−N(21)	2.100(7)
Cl(1)−V(1)−O(1)	99.5(1)	Cl(2)−V(2)−O(2)	99.1(1)
Cl(1)−V(1)−O(2)	80.5(1)	Cl(2)−V(2)−N(21)	89.5(2)
O(1)−V(1)−O(2)	180	O(2)−V(2)−N(21)	96.3(2)
Cl(1)−V(1)−N(11)	89.5(2)	Cl(2)−V(2)−Cl(2A)	161.9(1)
O(1)−V(1)−N(11)	94.5(2)	N(21)−V(2)−Cl(2A)	88.5(2)
O(2)−V(1)−N(11)	85.5(2)	Cl(2)−V(2)−O(1A)	80.9(1)
Cl(1)−V(1)−Cl(1A)	161.0(1)	O(2)−V(2)−O(1A)	180
Cl(1)−V(1)−N(11A)	89.1(2)	N(21)−V(2)−O(1A)	83.7(2)
N(11)−V(1)−N(11A)	171.1(3)	N(21)−V(2)−N(21A)	167.4(4)

[a] Estimated standard deviations in the least significant digit are given in parentheses.

The signal at each temperature consists of a single isotropic line with a peak to peak line width of 35(1) G and an approximately Lorentzian shape (optimal fitting of the lower temperature peak is achieved with a 70% Lorentzian/30% Gaussian line). These characteristics are typical of an exchange-narrowed spectrum arising from an extended array of exchange-coupled spins with the large admixture of Gaussian character to the line typical of a low-dimensional magnetic system.[18]

(18) (a) Abragam, A.; Bleaney, B. *Electron Paramagnetic Resonance of Transition Ions*; Oxford University Press: Oxford, U.K., 1970; pp 527−9. (b) Carlin, R. L. *Magnetochemistry*; Springer-Verlag: Berlin, 1986; Chapters 5,7.

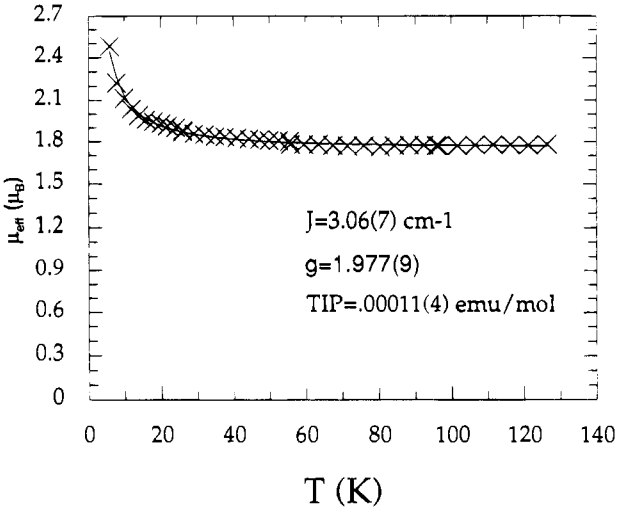

Figure 4. Plot of μ_{eff} versus temperature for **III**: experimental data (×); theoretical fit using parameters shown (—).

Table 9. Spin-Hamiltonian Parameters[a]

compd	medium	temp, K	$g_{\parallel}$	$g_{\perp}$	g_0	$A_{\parallel}$	$A_{\perp}$	A_0
						$cm^{-1} \times 10^4$		
I	water	RT			1.972			104
	water/glycerine	77	1.948	1.978	1.968	176	66	103
II	MeOH	RT			1.968			103
	MeOH/toluene	77	1.944	1.975	1.965	176	68	104
III	solid	RT			1.97			
	CH_2Cl_2/toluene	RT			1.979			92
		115	1.948	1.984	1.972	175	69	104
	ACN	115	1.947	1.965	1.959	170	64	100
	MeOH	115	1.948	1.984	1.972	175	69	105
	CH_2Cl_2	115[b]	1.961			70		
IV	CH_2Cl_2/toluene	RT			1.975			102
		115	1.951	1.987	1.975	177		104
V	CH_2Cl_2/toluene	RT	1.969	1.989	1.982	96	48	64
		115[c]	1.967	1.987	1.981	90	33	52

[a] Values of R were calculated from the following relationship for an axial dimer: $R = (0.65g^2/D)^{1/3}$; see ref 17b. [b] In the parallel region $D = 0.0186$ cm^{-1}, $R = 5.12$ Å; the perpendicular region was too complex to allow for evaluation of parameters. [c] D and R are respectively 0.0345 cm^{-1} and 4.20 Å for the parallel region and 0.0340 cm^{-1} and 4.19 Å for the perpendicular region.

Because of the potential for magnetic exchange interactions between the vanadium(IV) ions propagated by the bridging ligands, variable-temperature magnetic properties of compound **III** were investigated. The magnetic susceptibility data in the range 6−130 K for the compound follow Curie−Weiss behavior with $g = 2.019(2)$ and $\Theta = 3.2(2)$ K. The effective magnetic moment for the compound is 1.78 μ_B at 130 K and remains essentially constant in the higher temperature range (60−130 K) with a gradual and increasingly pronounced positive deviation as the temperature decreases, attaining a value of 2.48 μ_B at 6 K. These data were fit to the Fisher model for a Heisenberg chain (scaled to $S = {}^1/_2$)[18b] with excellent agreement between the experimental and calculated curves (Figure 4). Least-squares-fitting procedures gave the best-fit parameters of $J = 3.06(7)$ cm^{-1}, $g = 1.977(9)$, and TIP = 0.00011(4) cm^3 mol^{-1}, where J is the exchange coupling constant and TIP is the temperature-independent paramagnetism of the vanadium(IV) ion. The best-fit g value agrees very well with that determined experimentally for a powdered sample of the compound by EPR spectroscopy (Table 9). The magnetic properties of **III** describe a weak ferromagnetically coupled chain of vanadyl ions and are comparable to those observed in other compounds known to contain V=O···V chains such as [*N*,*N*′-propylenebis(salicylaldiminato)]oxovanadium(IV).[19]

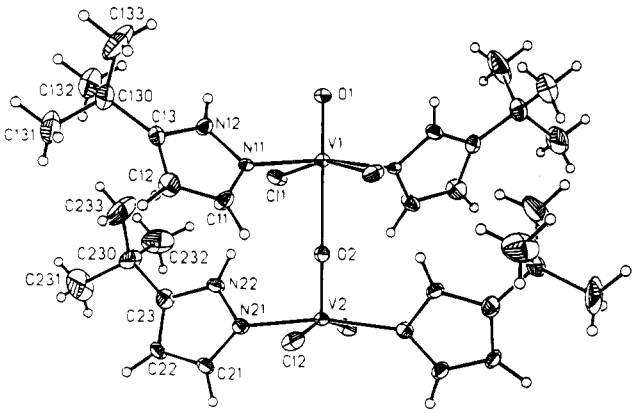

Figure 5. Thermal ellipsoid plot (30%) for **III** with atom-labeling scheme.

Despite the fact that head to tail solid state polymerization in **III** was indicated by the physical and spectroscopic data presented thus far, confirmation of this required a single-crystal X-ray analysis. Fortunately, after many unsuccessful attempts, we were able to obtain single crystals suitable for X-ray analysis via a thermal gradient method. The structure of **III** with the atom-labeling scheme is depicted in Figure 5, and selected bonding parameters are given in Table 8. The structure consists of (t-Bupz)$_2$VOCl$_2$ subunits packed such that the vanadyl oxygen atom of one subunit occupies the sixth coordination site of the vanadium atom in a neighboring subunit. This results in an infinite linear chain of vanadium atoms linked by V=O···V bonds in which the chain axis is coincident with the crystallographic 4_2 rotation axis. The atoms forming the basal planes in adjacent subunits are staggered relative to each other with a dihedral angle near 45°. This leads to the unique situation where the ligands spiral along the chain in a helical fashion, giving rise to a structure that resembles a protein α-helix. Like the protein structure, the helix in **III** is stabilized by hydrogen bonding, here between the free N−H in one subunit with a chloride ion in the subunit above it (Figure 6). The mean V=O bond length of 1.607(7) Å is within the 1.56−1.62 Å range normally observed in oxovanadium(IV) compounds.[20] The *tert*-butylpyrazole rings in **III** are planar within experimental error.

[(t-Bupz)$_4$VO(H$_2$O)]Cl$_2$, IV. From the filtrate that produced **III**, a second oxovanadium(IV) complex, **IV**, was isolated. Elemental analysis and UV−vis, IR, and EPR spectroscopy are all consistent with a six-coordinate structure. X-ray diffraction proved the compound to be [(t-Bupz)$_4$VO(H$_2$O)]Cl$_2$. The product does not show any evidence for intermolecular polymerization and displays a $\nu_{V=O}$ at about 976 cm^{-1} both in the solid state and in solution. The overall stoichiometry for the reaction that produces these two compounds is

$$O_2 + 6t\text{-Bupz} + 2VCl_3 \xrightarrow[\text{(or DMF)}]{\text{ACN}} (t\text{-Bupz})_2VOCl_2 + [(t\text{-Bupz})_4VO(H_2O)]Cl_2 + 2Cl^-$$

It is noteworthy that the same products are obtained whether t-Bupz or K[HB(t-Bupz)$_3$] is used as the starting material. This clearly indicates decomposition of the K[HB(t-Bupz)$_3$. The friability of the tris(pyrazolyl)borate class of ligand has been noted before, and a variety of decomposition modes have been observed.[21−26]

Table 10. Selected Bond Lengths (Å) and Bond Angles (deg) for **IV**[a]

V(1)−O(1)	1.580(9)	V(1)−O(2)	2.136(9)
V(1)−N(1)	2.118(7)	V(1)−N(3)	2.123(5)
V(1)−N(1A)	2.118(7)	V(1)−N(3A)	2.124(5)
O(1)−V(1)−O(2)	180	O(1)−V(1)−N(1)	93.7(2)
O(2)−V(1)−N(1)	86.3(2)	O(1)−V(1)−N(3)	94.7(2)
O(2)−V(1)−N(3)	85.3	N(1)−V(1)−N(3)	90.9(2)
O(1)−V(1)−N(1A)	93.7(2)	O(2)−V(1)−N(1A)	86.3(2)
N(1)−V(1)−N(1A)	172.7(5)	N(3)−V(1)−N(1A)	88.5(2)
O(1)−V(1)−N(3A)	94.7(2)	O(2)−V(1)−N(3A)	85.3(2)
N(1)−V(1)−N(3A)	88.5(2)	N(3)−V(1)−N(3A)	170.6(4)
N(1A)−V(1)−N(3A)	90.9(2)		

[a] Estimated standard deviations in the least significant digit are given in parentheses.

Figure 7 shows the atom-labeling scheme for the cationic portion of **IV**. The vanadium and two oxygens, one from the oxo group and the other from a coordinated water, lie on a crystallographically imposed 2-fold axis. The overall geometry about the vanadium is pseudooctahedral with the four *tert*-butylpyrazoles making up the equatorial plane and with the oxo group and the water occupying the axial positions. There are also two outer sphere chlorides as counterions and four acetonitrile solvent molecules per asymmetric unit. The chlorides are hydrogen-bonded to the N−H hydrogens of the pyrazoles and the coordinated water. Bond lengths and angles around the vanadium are unexceptional (Table 10) with the vanadium−nitrogen bonds averaging 2.120 Å and the V=O bond at 1.580(9) Å. As observed earlier for **II**, the V−OH$_2$ bond *trans* to the oxo group is also lengthened (2.136 Å) in **IV** relative to known *cis* vanadyl(IV) V−OH$_2$ bonds. The vanadium is very slightly displaced (0.155 Å) from the plane made up of the four equatorial nitrogens, and the pyrazole rings are tilted some 20° from vertical with the *tert*-butyl groups all pointing up toward the vanadyl oxygen. The lack of a solid state interaction in **IV** as compared to **III** is presumably due both to the increased steric interactions caused by the presence of four *tert*-butylpyrazole groups and to the presence of the capping water molecule, which effectively eliminates the open coordination site present in **III**.

(t-Bupz)$_2$VOCl$_2$(F)VOCl(t-Bupz)$_3$, V. Treatment of **III** or **IV** with silver perchlorate or nitrate resulted in the precipitation of silver chloride. The green solids isolated from these reactions gave infrared spectra virtually identical to those of the starting material, suggesting no major structural changes had occurred. However when either AgBF$_4$ or AgPF$_6$ was used to precipitate the chloride, a slight color change was noted. Crystallization of the crude product of the AgBF$_4$ reaction from methylene chloride/hexane at −20 °C gave large bright blue crystals of **V**. Both the presence of an intense EPR spectrum and a room-temperature moment near 1.7 μ_B indicated that the vanadium was still tetravalent. The observation of two sharp V=O stretches in the IR at 977 and 957 cm^{-1} and a forbidden "half-field" transition in the low-temperature EPR both pointed to an asymmetric dimeric structure (*vide infra*). Fortunately X-ray quality crystals were again forthcoming. Not unexpectedly, a single-atom-bridged dimer was revealed. What was surprising

(19) Drake, R. F.; Crawford, V. H.; Hatfield, W. E.; Simpson, G. D.; Carlisle, G. O. *J. Inorg. Nucl. Chem.* **1975**, *37*, 291.
(20) Chasteen, N. D.; Belford, R. L.; Paul, I. C. *Inorg. Chem.* **1969**, *8*, 408.
(21) Cano, M.; Heras, J. V.; Trofimenko, S.; Monge, A.; Gutierrez, E.; Jones, C. J.; McCleverty, J. A. *J. Chem. Soc., Dalton Trans.* **1990**, 3577.
(22) Alobaidi, N.; Jones, C. J.; McCleverty, J. A. *Polyhedron*, **1989**, *8*, 1033.
(23) Bradley, D. C.; Hursthouse, M. B.; Newton, J.; Walker, N. P. C. *J. Chem. Soc., Chem. Commun.*, **1984**, 188.
(24) Hughes, D. L.; Leigh, G. J.; Walker, D. G. *J. Chem. Soc., Dalton Trans.* **1988**, 1153.
(25) Khan, M. M. T.; Roy, P. S.; Venkatasubramanian, K.; Khan, N. H. *Inorg. Chim. Acta*, **1990**, *176*, 49.
(26) Cano, M.; Heras, J. V.; Santamaria, E.; Pinilla, E.; Monge, A.; Jones, C. J.; McCleverty, J. A. *Polyhedron*, **1993**, *12*, 1711.

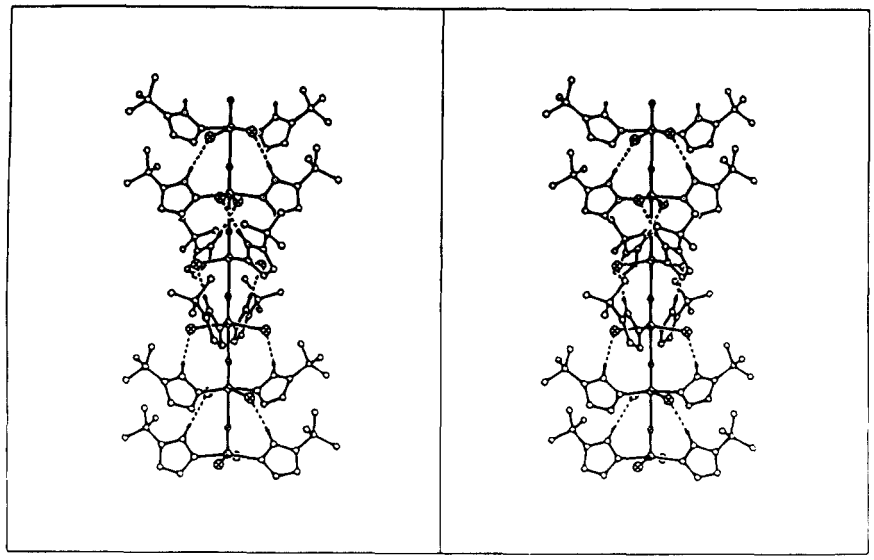

Figure 6. Stereoview of an illustration of the hydrogen bonding that stabilizes the helical, polymeric structure of **III**.

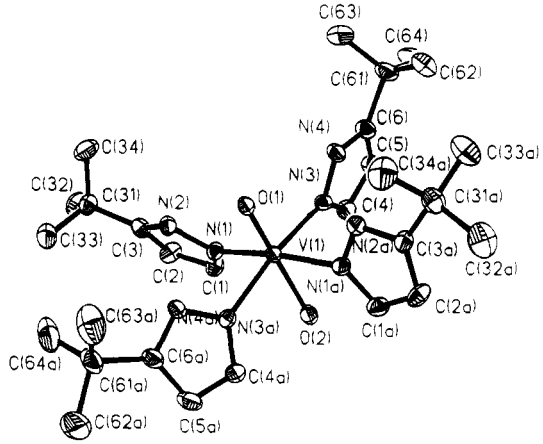

Figure 7. Thermal ellipsoid plot (30%) for the cationic portion of **IV** with atom labeling scheme.

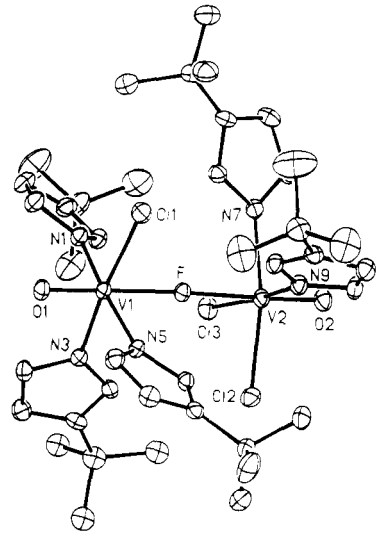

Figure 8. Thermal ellipsoid plot (30%) for **V** with atom-labeling scheme. For clarity, only one conformation of the disordered *tert*-butyl group attached to the N(3) pyrazole ring is shown.

was the fact that the bridging ligand was fluoride. Given the nature of the synthesis, the fluoride had to be abstracted from the BF_4^- anion, a situation not without precedence.[27,28]

Figure 8 shows the structure and atom-labeling scheme for **V**. Selected bond lengths and angles are shown in Table 11. Both vanadium atoms have octahedral coordination with the fluoride representing a shared vertex. The fluoride bridge is nearly linear with V(1)−F−V(2) angle of 175.8° although the two V−F bonds are inequivalent with V(1)−F shorter, 2.047-(2) Å, than V(2)−F, 2.109(2) Å. One vanadium fragment (V(1)) contains three pyrazoles and a chloride in the basal plane with an oxo group and a fluoride occupying the apical positions. The other fragment (V(2)) contains two pyrazoles and two chlorides in a *cis* arrangement in the basal plane. The atoms forming the basal planes in both subunits are staggered relative to each other with a dihedral angle near 45°. The *tert*-butyl groups of the pyrazoles all point away from the oxo groups, forming a protective cavity around the fluoride bridge, and each is locked into position by a NH···Cl hydrogen bond.

In frozen CH_2Cl_2/toluene, compound **V** presents an unusually well-resolved dimer spectrum with the high- and low-field transition envelopes for the parallel orientation found on the outer edges of the main spectrum and a readily observed "half-field" envelope from the forbidden $\Delta m_s = \pm 2$ transition at approximately 1600 G (Figure 9). Consistent with the dimeric nature of this compound, the observed hyperfine splitting is approximately half that for the mononuclear compounds (Table 9). Values for zero-field splitting in the spin triplet measured for both the parallel and perpendicular orientations, $D = 0.0345$ and 0.0340 cm^{-1} respectively, yield intradimer V···V distances of 4.21 and 4.19 Å, in good agreement with the 4.16 Å distance found in the crystal structure of **V**. Also observed are small splittings into doublets of the parallel components of the spectrum (on the order of 25 G) which we take to be superhyperfine coupling of the unpaired electron with the bridging $I = {}^1/_2$ ^{19}F nucleus. Room-temperature solution spectra are highly solvent dependent. In methanol an eight-line spectrum characteristic of mononuclear vanadium is found, the dimer evidently dissociating in polar solvents. In toluene a distinct 15-line spectrum is obtained with all the characteristics previously noted for an isotropic dinuclear vanadium compound.

The susceptibility data (6−250 K) for the dimer **V** closely follow Curie−Weiss behavior. A linear fit to a plot of χ^{-1} versus T yields best-fit parameters $C = 0.678(2)$ emu K mol^{-1}, $g = 1.904(3)$, and $\Theta = 2.03(4)$ K. The effective magnetic moment of **V** is about 1.65 μ_B at the higher temperature range. Below 100 K, however, the moment exhibits a small gradual increase to a value of 1.85 μ_B at about 6 K. These data are consistent with an uncoupled dimer throughout most of the

(27) Bochmann, M. *Angew. Chem., Int. Ed. Engl.* **1992**, *31*, 1181.
(28) Gorrell, I. B.; Parkin, G. *Inorg. Chem.* **1990**, *29*, 2452.

Table 11. Selected Bond Lengths (Å) and Bond Angles (deg) for **V** and **VI**[a]

	Compound **V**		
V(1)–Cl(1)	2.380(1)	V(1)–F	2.047(2)
V(1)–O(1)	1.590(3)	V(1)–N(1)	2.119(3)
V(1)–N(3)	2.103(3)	V(1)–N(5)	2.116(3)
V(2)–Cl(2)	2.395(1)	V(2)–Cl(3)	2.371(1)
V(2)–F	2.109(2)	V(2)–O(2)	1.588(3)
V(2)–N(7)	2.119(3)	V(2)–N(9)	2.130(3)
Cl(1)–V(1)–F	84.4(1)	Cl(1)–V(1)–O(1)	96.1(1)
F–V(1)–O(1)	179.4(1)	Cl(1)–V(1)–N(1)	91.1(1)
F–V(1)–N(1)	85.5(1)	O(1)–V(1)–N(1)	94.1(1)
Cl(1)–V(1)–N(3)	171.7(1)	F–V(1)–N(3)	87.6(1)
O(1)–V(1)–N(3)	91.9(1)	N(1)–V(1)–N(3)	85.8(1)
Cl(1)–V(1)–N(5)	90.2(1)	F–V(1)–N(5)	87.3(1)
O(1)–V(1)–N(5)	93.1(1)	N(1)–V(1)–N(5)	172.5(1)
N(3)–V(1)–N(5)	91.9(1)	Cl(2)–V(2)–Cl(3)	91.4(1)
Cl(2)–V(2)–F	83.1(1)	Cl(3)–V(2)–F	87.1(1)
Cl(2)–V(2)–O(2)	99.0(1)	Cl(3)–V(2)–O(2)	97.2(1)
F–V(2)–O(2)	175.2(1)	Cl(2)–V(2)–N(7)	166.7(1)
Cl(3)–V(2)–N(7)	90.6(1)	F–V(2)–N(7)	83.9(1)
O(2)–V(2)–N(7)	93.8(1)	Cl(2)–V(2)–N(9)	90.3(1)
Cl(3)–V(2)–N(9)	171.7(1)	F–V(2)–N(9)	85.0(1)
O(2)–V(2)–N(9)	90.7(1)	N(7)–V(2)–N(9)	86.0(1)
V(1)–F–V(2)	175.8(1)		
	Compound **VI**		
V(1)–F(1)	2.190(6)	V(1)–O(1)	1.705(13)
V(1)–O(2)	1.638(12)	V(1)–N(11)	2.125(14)
V(1)–N(21)	2.061(13)		
F(1)–V(1)–N(11)	86.5(5)	F(1)–V(1)–O(2)	125.6(6)
N(11)–V(1)–O(2)	90.7(6)	F(1)–V(1)–O(1)	119.4(6)
N(11)–V(1)–O(1)	89.7(6)	O(2)–V(1)–O(1)	114.9(6)
F(1)–V(1)–N(21)	92.6(5)	N(11)–V(1)–N(21)	177.6(6)
O(2)–V(1)–N(21)	91.6(6)	O(1)–V(1)–N(21)	88.8(6)

[a] Estimated standard deviations in the least significant digit are given in parentheses.

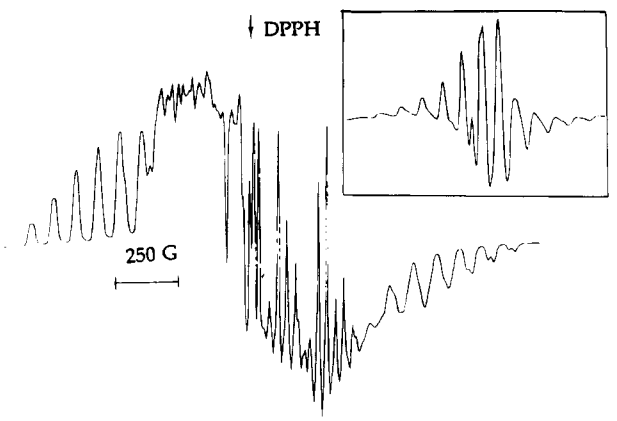

Figure 9. X-band EPR spectrum of **V** in frozen CH_2Cl_2/toluene glass at 115 K. Conditions: 9.43 GHz frequency, 2 mW power, 6.0 G modulation amplitude, 2 × 10^4 gain, 2500 G scan range, 3 min scan time. The insert shows the "half-field" transition. The receiver gain for this trace was 10 times greater than that used for the main trace.

temperature range, with the small increase of the moment at low temperature possibly resulting from a weak ferromagnetic intradimer exchange coupling. This result would be in agreement with previous observations of weak ferromagnetic intradimer exchange coupling in related oxovanadium tartrate systems where the magnetic orbital (d_{xy}) is also perpendicular to the dimer axis.[29] Weiss constants for the tartrate dimers, however, are negative, although this probably results from relatively strong antiferromagnetic interdimer interactions. The present dimer is substantially more voluminous and would have, presumably, interdimer exchange weak enough for the intradimer exchange to be dominant. A fit of the μ_{eff} versus temperature curve to the Bleaney–Bowers equation[18b] yields J = 3.0(4) cm^{-1} and g = 1.902(6).

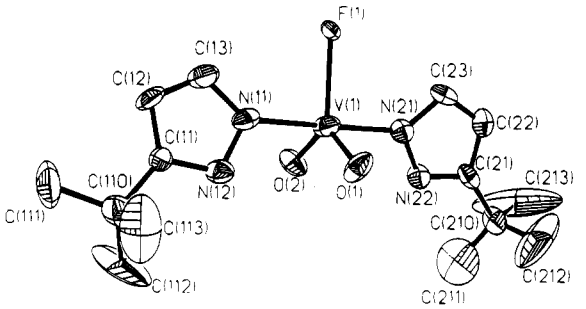

Figure 10. Thermal ellipsoid plot (30%) for **VI** with atom-labeling scheme.

(*t*-Bupz)$_2$VO$_2$F, VI. Allowing a methylene chloride solution of **V** to stand in the air for long periods of time resulted in the appearance of several other fluoro-containing vanadium pyrazole complexes. Unfortunately these complexes appeared as complicated mixtures which resisted purification efforts or attempts at rational synthesis. However, pale greenish yellow crystals of **VI** were physically separated from crystals of **V** and another unknown deep blue material and subjected to single-crystal X-ray analysis. The complex proved to be a mononuclear vanadium(V) species, (*t*-Bupz)$_2$VO$_2$F. Selected bond lengths and angles are given in Table 11, and an ORTEP diagram showing the atom-labeling scheme is shown in Figure 10. The presence of fluoride in the product once again underscores the avidity of high-valent vanadium for this element. The pervanadyl unit in **VI** adopts a trigonal bipyramidal (TBP) geometry with *tert*-butylpyrazoles in the apical positions and the oxo groups and the fluoride in equatorial sites. The vanadium–oxygen bonds in **VI** are slightly elongated (mean V=O is 1.671 Å) from what is typical in pervanadyl complexes due to the formation of strong hydrogen bonds between the N–H hydrogens and the oxo groups on neighboring molecules (mean O···H = 1.969 Å and O–H–V angles of 147°), resulting in the formation of weakly linked dimers. Although the quality of the structure is reduced somewhat by disorder in the *tert*-butyl groups, other bond lengths and angles seem unexceptional.

Discussion

While vanadyl complexes are most frequently five-coordinate, adopting a square pyramidal geometry, many examples of six-coordinate species are known as well. The compounds presented in this study represent a particularly interesting series showing as they do three distinct ways that a pentacoordinate vanadyl ion can achieve a higher coordination number. These include intermolecular axial interactions such as those seen in **III**, addition of a sixth ligand (either neutral or anionic) as in **I**, **II**, and **IV**, or dimerization via a bridging atom as in **V**. Also evident is the rather unexpected avidity of vanadium for the fluoride anion as a ligand as evidenced by the removal of fluoride from either BF_4^- or PF_6^- anions.

There are two major factors that seem to control the nature of the products isolated in this work. One of these is the steric aspects of the pyrazole ligands. With the unsubstituted pyrazole only the tetrakis(pyrazole) complex could be isolated. Conversely with the 3,5-dimethylpyrazole the only isolable product was the bis species. In the case of the 3(5)-*tert*-butylpyrazole both structural types could be isolated. This suggests that the 3,5-dimethyl is the most sterically demanding of the three pyrazoles with the mono-*tert*-butyl derivative adopting an

(29) (a) Wrobleski, J. T.; Thompson, M. R. *Inorg. Chim. Acta* **1988**, *150*, 269. (b) Crawford, V. H.; Hatfield, W. E.; Tapscott, R. E. *J. Mol. Struct.* **1977**, *38*, 141. (c) Carlisle, G. O.; Simpson, G. D. *J. Mol. Struct.* **1975**, *25*, 219.

intermediate position. This ordering is also reflected in the average tilt angle of the pyrazoles from vertical (vertical being defined along the V=O bond vector) with angles of 1.65° for the unsubstituted pyrazole, 22.3° for the 3(5) *tert*-butyl, and 37.7° for the 3,5-dimethylpyrazole complexes. Since π-bonding should decrease with increasing twist angle up to 45°, one might have expected this to be reflected in V−N bond lengths. No such trend is evident however as these bond lengths are all within 0.03 Å of each other. This suggests that π-bonding is relatively unimportant and that the pyrazoles are acting as pure σ donors in these molecules.

The other important aspect is stabilization of the observed structures by formation of strong intra- or intermolecular hydrogen-bonding networks. For example, in **III** the *tert*-butyl groups and the uncoordinated nitrogen atoms all point up toward the vanadyl oxygen and are locked into position by intramolecular hydrogen bonds involving the NH hydrogen in one subunit with a chlorine atom in the next (upper) subunit, thereby stabilizing the polymeric chain. Hydrogen bonding has been found to impart stability to polymer formation in $VO(acac)_2(p\text{-}O_2NC_6H_4OH)$ as well.[30] This increased stability is reflected in the mean O···V bond length of 2.313(7) Å in **III** which, with one exception, is considerably shorter than that found in other characterized solid state polymers of this type.[30−33] For example, **III** can be compared to the related pyridine compounds $(py)_2VNCl_2$ and $(py)_2VOCl_2$. These are also both linear chain polymers composed of six-coordinate vanadium atoms linked by alternating short and long vanadium−oxygen/nitrogen bonds. They lack the free NH hydrogen, however, and are therefore unable to engage in intramolecular hydrogen bonding. The lack of this extra stabilization results in "bonds" (2.588(9) Å for the O···V in $(py)_2VOCl_2$[33] and 2.729(7) Å for N···V in the nitride[32]) that are so long that the vanadium atom could be considered to be five-coordinate. In view of the weak N···V interactions, Doherty *et al.*[32] proposed that interchain pyridine $\pi-\pi$ interactions are crucial to the stability of the polymeric structure of these compounds.

The isolation of **II** as a mononuclear species was somewhat surprising since the vanadium coordination sphere of $(3,5\text{-}Me_2pz)_2VOCl_2$ is the same as that of a subunit of **III**. However, due to steric crowding resulting from the two methyl substituents on the pyrazole ring, "head-to-tail" polymer formation is impossible. A dimeric molecule, $[(3,5\text{-}Me_2pz)_2VOCl_2]_2$·THF, with much the same vanadium coordination sphere has previously been obtained from the decomposition of $K[HB(3,5\text{-}Me_2pz)_3]$ during reaction with VCl_3 in THF.[1] In this case, however, the uncoordinated nitrogen atoms in the two subunits point toward each other, making the extended NH···Cl hydrogen bonding seen in **III** impossible but still allowing stabilization of the dimer.

Finally, we come to compounds **I** and **IV**, each of which contains the same types of ligands: four pyrazoles, two chlorides, one oxo oxygen, and one water. In **IV**, the two chloride ions are outside the coordination sphere of the vanadium whereas, in **I**, one chloride and a water molecule are outside the metal coordination sphere. **I** and **IV** can therefore be classified as ionization isomers. In **I**, the hydrogen bonding between the outer sphere chloride, the lattice water, and the free N−H protons result in weakly linked, discrete "head-to-head" dimers. In **IV**, however, the hydrogen-bonding network between similar units leads to a "head-to-tail" uniaxial polymeric interaction similar to, but much weaker than, that seen in **III**. While the factors that stabilize one isomer over the other are not readily apparent, presumably both the steric demands of the ligands and hydrogen-bonding interactions play significant roles.

Acknowledgment. This work was supported by Robert A. Welch Foundation Grant AI-1157, Grant 3615-002 from the Texas Advanced Research Program and National Institutes of Health Grant GM4767601 to Carl J. Carrano. NSF-ILI Program Grant USE-9151286 is acknowledged for support of the X-ray diffraction facilities at Southwest Texas State University. The authors also wish to thank Dr. J. D. Korp, Department of Chemistry, University of Houston, for assistance with data collection and analysis of **V**.

Supplementary Material Available: Listings of detailed crystallographic data, anisotropic thermal parameters, idealized hydrogen atom parameters, and detailed bond lengths and angles for all compounds (37 pages). Ordering information is given on any current masthead page.

IC940899J

(30) Taguchi, H.; Isobe, K.; Nakamura, Y.; Kawaguchi, S. *Bull. Chem. Soc. Jpn.* **1978**, *51*, 2025.

(31) The lone exception is the 2.213(9) Å V···O bond length found in [*N*,*N*′-propylenebis(salicylaldiminato)]oxovanadium, VO(salpn), where strong intrachain π-stacking stabilizes the polymer. See ref 11.

(32) Critchlow, S. C.; Lerchen, M. E.; Smith, R. C.; Doherty, N. M. *J. Am. Chem. Soc.* **1988**, *110*, 8071.

(33) Hills, A.; Hughes, D. L.; Leigh, G. J.; Prieto-Alcon, R. *J. Chem. Soc., Dalton Trans.* **1993**, 3609.